Analysing a TiEMPO simulation of a DESHIMA 2.0 observation of the dusty starburst galaxy HFLS3

A. Doing

Technische Universiteit Delft

Analysing a TiEMPO simulation of a DESHIMA 2.0 observation of the dusty starburst galaxy HFLS3

by

A. Doing

to obtain the degree of Bachelor of Science
at the Delft University of Technology,
to be defended publicly on Tuesday August 31, 2021 at 09:00 AM.

Student number:	4453972	
Project duration:	November 1, 2020 – August 31, 2021	
Thesis committee:	Dr. A. Endo,	TU Delft
	Dr. M. B. van Hoven,	TU Delft
	Dr. A. J. L. Adam,	TU Delft
	Prof. dr. ir. A. W. Heemink,	TU Delft

Credits of the front page picture: Artist's impression of the dusty starburst galaxy HFLS3 from [1].

An electronic version of this thesis is available at `http://repository.tudelft.nl/`.

TU Delft

Abstract

Observing dust obscured high redshift galaxies is vital to understand the evolution of the early universe and the formation of stars and galaxies. HFLS3 is such a galaxy, and its emission spectrum can be detected at submillimeter wavelengths. With the Deep Spectroscopic High-redshift Mapper 2.0 (DESHIMA 2.0) it is possible to observe these high redshift galaxies at the ASTE telescope in Chile. With the recently developed Time-dependent End-to-end Model for Post-process Optimization (TiEMPO) it is possible to simulate observations of DESHIMA2.0.

With TiEMPO it is possible to simulate different sky positions to accommodate different scenarios of wind direction. However, since TiEMPO is fairly new there are still some problems with the simulation of several of the the possible sky positions. More importantly, the model has to be tested with realistic high-redshift sources that are interesting for observations with DESHIMA 2.0. To predict whether a source can be observed with DESHIMA 2.0 it is necessary to estimate what the signal to noise ratio will be. Parameters like the precipitable water vapor and the observation time determine if a source can be measured.

In this report, a solution is introduced to make it possible to use 6 different sky positions while simulating DESHIMA 2.0 measurements with TiEMPO. This solution is part of the current TiEMPO version, and can be used in future simulations.

With the improved model we simulate an observation of the dusty starburst galaxy HFLS3. The CII line in the emission spectrum is fainter than simulations done so far. A new model to simulate the emission spectrum was made to accommodate for this. With the use of beam switching some of the noise from the atmosphere is removed from the data. The simulation is compared to previously made observations as described in [2]. From the resulting signal we calculate the standard deviation σ to determine the signal to noise ratio (SNR). The values found for σ correspond well with the expected relation between σ and integration time. We say that a emission line is detected if the SNR is greater than 5. The calculated SNR of a 16 hour observation with a pwv value of 1.0 mm is 5.2, which shows that HFLS3 can be detected with DESHIMA 2.0. Two simulations of 8 hours with pwv values of 1.0 and 0.5 mm are compared as well. After 8 hours of observation, the SNR is 3.9 for a pwv value of 1.0 mm and 6.0 for a pwv value of 0.5 mm. With this lower pwv value the galaxy can be detected after 8 hours.

The analysis of this project can be repeated on other sources to make a database for future DESHIMA 2.0 simulations. Hereby it is key to have models which can predict the emission lines of a galaxy accurately.

Contents

1

Introduction

People have always been interested in acquiring knowledge. We already know a lot about our own surroundings and are therefore looking further out into the universe to see what else we can learn. One of the things we are interested in are galaxies. The one we know best is our own milky way, but there are trillions more [3], and can have different shapes and contents. We want to observe galaxies because we can learn a lot about the origin of our own planet and solar system by observing them. We are particularly interested in distant galaxies. This is because the light in the universe has to travel trough space, which takes time. Therefore, when the light a galaxy emits arrives at Earth, observing this light is like looking back in time to when this light was emitted. The further a galaxy is away from us, the longer it has been since that light was emitted. For that reason distant galaxies can tell us a lot about the beginning and the evolution of the universe. Furthermore, star formation in galaxies is the reason galaxies gained their stellar mass and heavy elements. More research into star formation can provide us with answers as to how, for example, planets were formed [4].

It remains unknown how long after the big bang intense star formation occurred. We do know galaxies often go through a heavy star forming phase [5]. When stars are formed clouds of dust emerge. These dust particles make it difficult to observe a galaxy, since they absorb the optical and ultraviolet light emitted by the starts. This light is then emitted in the submillimeter range. When a galaxy is in this phase it is called a Submillimeter Bright Galaxy (SMG).

Observing SMGs can be done with the Atacama Submillimeter Telescope Experiment (ASTE), which is a submillimeter telescope located in Chile, see Figure 1.1.

Figure 1.1: The Atacama Submillimeter Telescope Experiment (ASTE) located in Chile. This image is from the National Astronomical Observatory of Japan (NAOJ).

It's goal is to measure submillimeter waves of the southern sky. The telescope is located in the Atacama desert in Chile, where the atmosphere has some excellent conditions. This matters because the water vapor in the Earths atmosphere absorbs radiation within the submillimeter wavelengths, which complicates the measurements. In the Atacama desert the air is cold and dry, and because of the altitude there is even less water vapor in the air. Still, there is significant absorption of the submm wavelengths during the measurements. In order to partly overcome this we can measure different positions in the sky. These positions overlap well in the atmosphere region, but at the location of the galaxy, the beams don't overlap at all. In Figure 1.2 you see an illustration of the beams in the atmosphere region and far away. The idea is that in one beam you have a galaxy, while the other beam measures the cosmic background. Both beams do contain a similar atmosphere emission, since the beams overlap well in this region. When we subtract the two signals from each other, only the galaxy measurement will remain. This is called sky chopping.

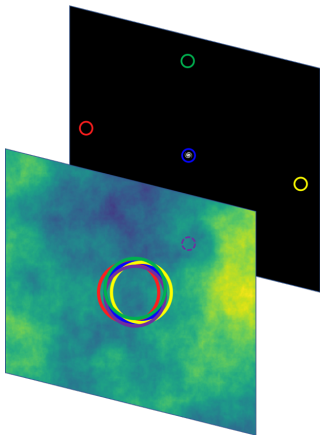

Figure 1.2: An illustration of different sky positions in the near-field (coloured square) and far-field (black square) of the telescope. The blue position in the centre contains the galaxy. The four surrounding positions don't contain a galaxy. This image is obtained from [6].

Within ASTE the Deep Spectroscopic High-Redshift Mapper 2.0 (DESHIMA 2.0) can be installed. DESHIMA 2.0 is an spectrometer and its main goal is to detect SMGs. It covers a wide frequency bandwidth of 220-440 GHz. Doing measurements with DESHIMA 2.0 is costly and takes a lot of time. Therefore it is vital to estimate beforehand what kind of measurements can be done and how significant the results will be. To be able to

make predictions of measurements, TiEMPO was developed. TiEMPO stands for Time-dependent End-to-end Model for Post-process Optimization, and is only recently developed [7]. It's a program which requires an input spectrum with which it simulates a DESHIMA measurement. The program is quite new and has yet to be tested with galaxies that are interesting for observations. In March 2022 the DESHIMA 2.0 chip will be tested in Chile. Simulations with TiEMPO can prove to be useful for these measurements. With realistic simulations it is possible to determine parameters such as observation time for interesting sources beforehand. This way the observations can be done more efficient saving time and money.

The goal of this report is to determine if we can measure the dusty starburst galaxy HFLS3 with DESHIMA 2.0. Therefore, we will first go into some of the theory of observing high-redshift galaxies. The necessary knowledge regarding some properties of galaxies will be discussed, after which we go into more detail regarding the challenges of observations. In the second chapter we discuss TiEMPO and the current difficulties with this program. We take a look into the global layout of the program and introduce a solution for one of the issues encountered. More specifically, a fix is explained which makes it possible for TiEMPO to simulate measurements for multiple sky positions. This makes it possible to do sky chopping in multiple directions.

In the third chapter we look into a full TiEMPO simulation of the dusty starburst galaxy HFLS3. The simulation of the galaxy spectrum is improved to accurately predict the signal from the galaxy. The signal to noise ratio over time is calculated to see under which circumstances this galaxy can be detected with a DESHIMA2.0 measurement. In chapter 4 we finish this report with conclusions and ideas for future prospects.

2

Observing Galaxies

In order to observe a galaxy it is important to understand how we measure galaxy signals on Earth, and which parts of this signal we are interested in. This chapter describes what the emission spectrum of a galaxy looks like, and how we can detect the redshift of a galaxy. Then some of the challenges we face during observations are explained, of which several can be partially resolved with the use of DESHIMA 2.0.

2.1. Emission spectrum

Galaxies consist of stars, gas and dust which are held together by gravity [8]. These components emit light which we can measure on Earth. This light spectrum is called the emission spectrum of a galaxy. An example can be found in Figure 2.1. This spectrum can be looked at in two parts; the continuum and the line emissions.

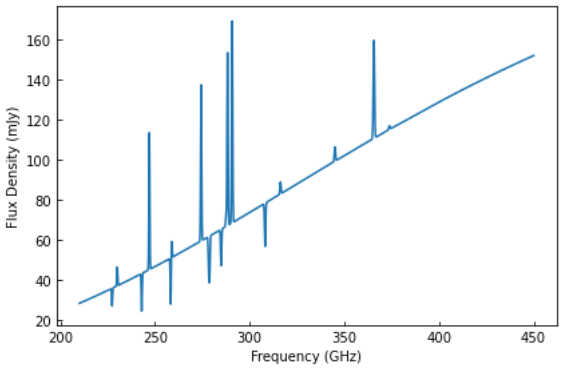

Figure 2.1: An example of an observed emission spectrum of a high redshift galaxy. On the x-axis is the frequency in GHz and on the y-axis the flux density in mJy.

2.1.1. Continuum

The continuum is the base line in the emission spectrum, and comes from the dust within a galaxy. Because of their heat, these dust particles emit far-infrared waves and act as a black body. With the telescope we can measure this radiation. The spectral radiance of a black body with temperature T and frequency f can be calculated using

$$B_f(f,T) = \frac{2hf^3}{c^2} \frac{1}{e^{\frac{hf}{k_B T}} - 1} \tag{2.1}$$

with $B_f(f,T)$ the spectral radiance in [W sr^{-1} m^{-2} Hz $^{-1}$], also called the specific intensity, f the frequency of the electromagnetic radiation and T the absolute temperature of the body. The constants are c the speed of light in a vacuum, h the Planck constant and k_B the Boltzmann constant. The radiation is not dependent on the shape of the object, which is very convenient since galaxies can have different shapes.

Ultimately we are interested in the luminosity or the flux density of the galaxy. Luminosity (L) is the total power emitted by an object, integrated over all angles and a predetermined frequency range. The units are W, but values are often normalised to the solar luminosity $L_\odot = 3.828 \cdot 10^{26}$ W. Since we cannot measure all around our desired object we cannot measure the luminosity directly, but it can be derived from the measured specific intensity. The specific intensity can be converted to flux density F_f, which is the power passing trough a surface per unit area per unit bandwidth, according to equation 2.2. Here we assume that the source fits completely in the beam of the telescope.

$$F_f = I_{f,source}\Omega_{source} \tag{2.2}$$

The units of F_f are W m^{-2} Hz$^-$1, but generally expressed in Jansky [Jy]. 1 Jy = 10^{-26} W m^{-2} Hz^{-1}. Ω_{source} is the solid angle of the source in sr. The solid angle of an object is the portion of a unit sphere that is covered when you look at the object from the centre of the sphere, as portrait in Figure 2.2.

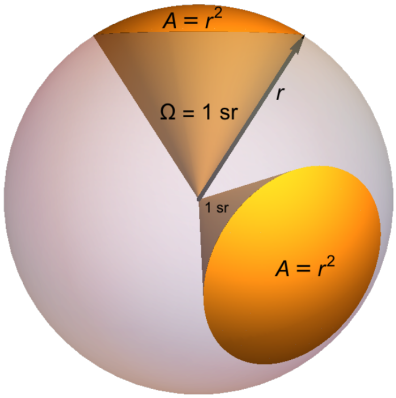

Figure 2.2: The solid angle is 1 sr if the area on a sphere is equal to the square of the radius. The image is made by [9].

From this we can calculate the flux F in units W m^{-2} which is the power passing trough a surface per unit area for the same predetermined frequency range. This can be converted to the luminosity. We approximate the galaxy as an isotropic source, thus we can use equation 2.3.

$$L = 4\pi F D_L^2 \tag{2.3}$$

With L the luminosity, F the flux and D_L the luminosity distance determined using [10].

For certain tests it is common to express the signal in temperature. The reason for this is that thermal radiators are used quite often in experiments because they are easy to prepare with good absolute accuracy. For our measurements we can express the power in sky brightness temperature T_{sky}: the physical temperature of a black body that would have the same intensity as the semitransparent sky [11]. T_{sky} can be calculated using the Johnson-Nyquist formula as in Formula 2.4.

$$T_{sky} = \frac{hf}{k_B \ln(\frac{hf}{psd+1})} \tag{2.4}$$

Where f is the frequency in Hz, psd the power spectral density in W Hz$^-$1 and λ the wavelength in m. k_B is the Boltzmann constant and h the Planck constant.

2.1.2. Emission and absorption lines

The other elements in the emission spectrum are the emission and absorption lines. Atoms can emit and absorb light of specific wavelengths. When an element is plentiful present in a galaxy the emission line is bright enough and becomes visible during the measurements of the emission spectrum. Next to the brightness of an emission line, the Full Width Half Maximum (FWHM) is very important to see if a line can be detected. It is an indication for the width of a peak. At FWHM the power of the peak is half of its maximum power.

CII line
Carbon (C) is an atom which is very useful for observing galaxies, particularly for star forming ones. Due to the photoelectric effect the light of stars will cause the surrounding dust particles to emit electrons. These electrons heat up gas, in galaxies particularly hydrogen gas, which can excite carbon atoms by colliding with them. Once a atom is in the excited stage the electrons within fall back and hereby emit photons with a wavelength of $158\mu m$, which corresponds to a frequency of $1900.5GHz$. The CII emission line is generally the brightest emission line in star forming galaxies [12], making it the best candidate to determine several properties of a SMG. There are different models to predict the brightness and FWHM of the CII line. Within this report we use CII lines based on [13] and [14].

CO line
Besides the CII line, we are also interested in the emission lines of carbon monoxide (CO). The advantage of the frequency of these lines is that there are multiple linearly spaced lines coming from the CO molecule. So we can use not only the frequency and FWHM of a emission line, but also the frequency difference between multiple lines to determine the redshift. The disadvantage of the CO lines is that they are less bright than the CII line and therefore more difficult to detect.
Next to the emission lines, there are also absorption lines visible in Figure 2.1. Absorption lines can be produced when photons from a hot source pass trough cold gas surrounding the galaxy. The gas absorbs atoms and re-emit them in random directions.

2.1.3. Redshift
Because the universe is expanding, objects that are not bound to us will move away from us. Consequently, we have a phenomenon called redshift. A galaxy emits light with a certain wavelength. If the galaxy wouldn't expand this light would arrive on Earth with the same wavelength. Because the universe does expand, the light that we observe on Earth has a longer wavelength than originally emitted. On the electromagnetic spectrum as seen in Figure 2.3 this means light will move to the red side of the spectrum, hence the name redshift.

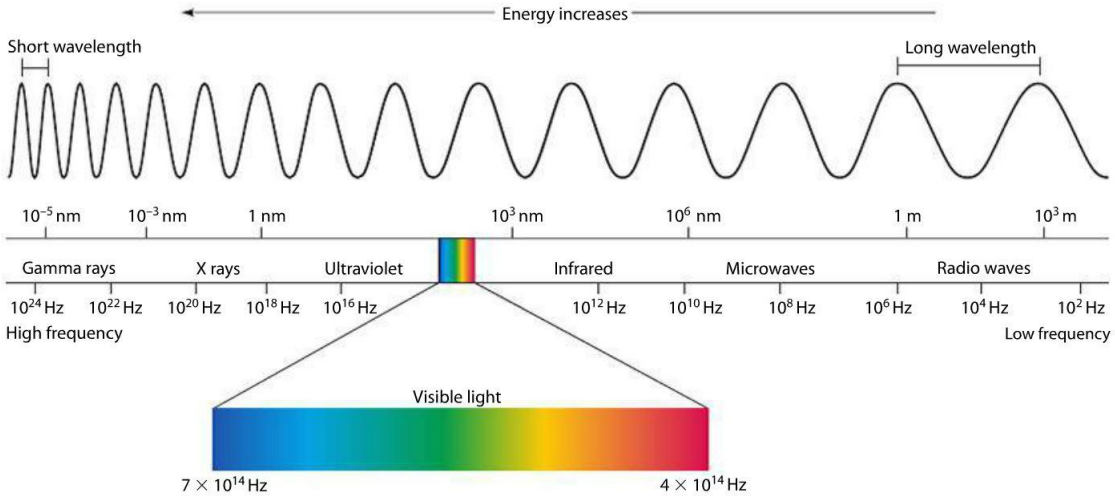

Figure 2.3: The electromagnetic spectrum with the values for wavelength in nm and the corresponding frequency values in Hz. This image is from [15].

Since we know the original wavelength of the emitted light of an atom, we can calculate the redshift of a galaxy with the observed wavelength of an emission line if we know which atom it belongs to. The redshift is related to the frequency as in equation 2.5 where z is the redshift, f_{emit} the frequency as emitted by the galaxy and $f_{observe}$ the frequency we observe at Earth.

$$1 + z = \frac{f_{emit}}{f_{observe}} \tag{2.5}$$

The redshift is related to the distance of an object in space. The further away an object is, the larger the red-

shift will be.

A difficulty about redshift is that with different redshift, emission lines can be measured at different places in the electromagnetic spectrum. Therefore, we need a spectrometer with a wide bandwidth to cover the entire frequency range where an emission line can end up.

2.1.4. Doppler broadening

An atom emits photons with very similar wavelengths, so originally the emission lines are relatively sharp peaks. However, when we observe the lines on Earth they are wider. A reason for this is that galaxies rotate, causing Doppler broadening. The broadening depends on the angle of inclination of the axis of rotation and the rate of rotation. The motion of individual atoms contribute to Doppler broadening as well. This broadening is for example influenced by the temperature, which differs between certain kind of atoms. The change in $FWHM$ can be calculated with equation 2.6.

$$\Delta f_{FWHM} = \sqrt{\frac{8k_B T ln(2)}{mc^2}} f_{rest} \tag{2.6}$$

with f_{FWHM} the frequency of the $FWHM$, T the temperature and m the mass of the emitting particle. All lines of a galaxy share the same redshift, but Doppler broadening can influence lines separately. When an emission line is broader it is harder to detect since the power will be distributed over a lager frequency range.

2.1.5. Dusty Star Forming Galaxies

As mentioned earlier there are different types of galaxies. Submillimetre-bright galaxies (SMGs) at high redshift are the most luminous, heavily star-forming galaxies in the Universe [16]. Several high redshift SMGs have been detected [17], but there is still much to learn from observing them. They have an important role in understanding the evolution of massive galaxies in the universe. In the analysis part of this report we look further into the dusty starburst galaxy HFLS3. This is a massive starburst galaxy at high redshift ($z = 6.43$) [2].

2.2. Observations

Besides the challenges we face from the universe itself, the fact that we want to observe galaxies on Earth brings along other difficulties. The main goal during observations is to measure objects with as less noise as possible. There are several different noise sources we have to take into account.

2.2.1. Atmosphere

When we observe radiation form the universe it passes trough our atmosphere. Unfortunately, the atmosphere emits radiation which is brighter than the galaxies we are interested in. Moreover, as mentioned in the introduction, the water vapor in the Earths atmosphere absorbs radiation within the submm wavelengths which distorts the measurements.

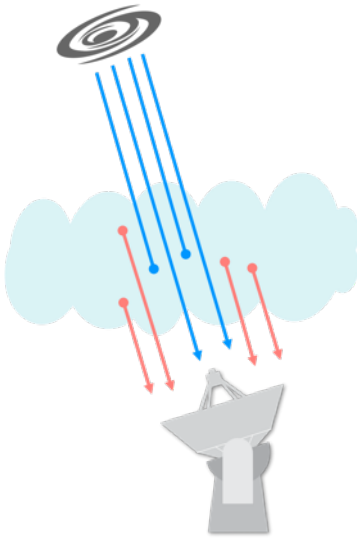

Figure 2.4: An illustration of the effect from the atmosphere to measurements of galaxies with a telescope on Earth. The red lines are the emission from the atmosphere. The blue lines are the signal from the galaxy, which can be absorbed by the atmosphere before it reaches the telescope.

To minimise the atmosphere interference the location of our measurements is very important. This is the reason the ASTE telescope in Chile is such a popular side for astronomers. The cold desert climate ensures there is little water vapor in the air, making it the driest non-polar desert in the world [18]. The height of the telescope also provides thinner air with less moisture. However, even at the best sites for submm astronomy, the brightness temperature of the atmosphere can be $10^3 - 10^5$ times stronger than the astronomical signal [7]. There are techniques to remove the emission from the measurements and retrieve the signal.

AB chopping

One of the techniques to remove the atmosphere emission is AB chopping, already briefly explained in the introduction. With AB chopping you measure two different sky positions. These positions overlap well in the atmosphere region, but are completely different in the far field. When we subtract the two signals from each other, ideally only the galaxy measurement will remain.

Transmittance

Unfortunately, the transmission is so bad in certain frequency bands that even with AB chopping the signal cannot be recovered. Figure 2.5 shows a model for the atmosphere transmittance for a precipitable water vapor (pwv) value of 1.0 mm. The pwv is the height of the water column that would be obtained if all water vapor would precipitate as rain.

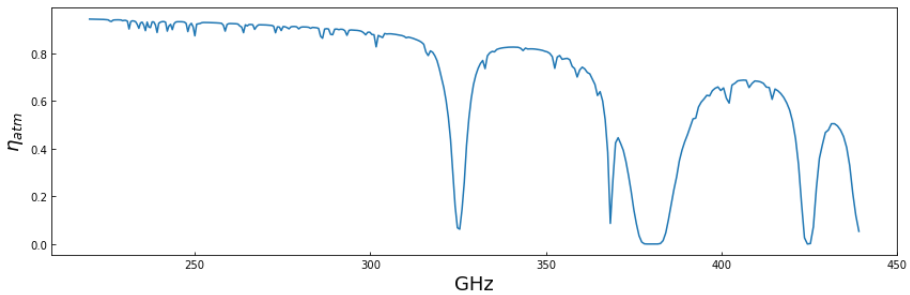

Figure 2.5: A simulation of the atmosphere transmittance vs the frequency in GHz for an precipitable water vapor value of 1.0 mm.

With the atmosphere transmittance we can calculate the atmosphere-corrected antenna temperature $T_A^* = T_{sky}/\eta_{atm}$ which corrects the measurements for the atmosphere transmittance. Around certain frequencies, for example at 380 GHz, the transmittance is almost zero. No matter how bright the source at this point, it

will not be possible to retrieve the signal. Furthermore, Figure 2.5 shows a constant transmittance for each frequency. The transmittance does however change over time during an observation depending on the pwv value. The time variation results in atmospheric noise. Because of these fluctuations over time, AB chopping needs to be done fast otherwise the atmosphere between the two positions is different.

2.2.2. Photon noise

Next to noise from the atmosphere we also have to take into account the photon noise, which consists of Poisson and photon bunching noise. Poisson noise originates from the random arrival time of photons. The number of photons N measured by a sensor over time interval t can be described by the Poisson distribution

$$Pr(N = k) = \frac{e^{-\lambda t}(\lambda t)^k}{k!} \tag{2.7}$$

where λ is the expected number of photons per time interval. The detectors in our spectrometer measure the arrival of photons over a given time interval, and the independent arrival of random individual photons lead to noise. A property of the Poisson distribution is that its variance is equal to its expectation, $E[N] = Var[N] = \lambda t$. This shows that photon noise is signal dependent, and that its standard deviation grows with the square root of the signal [19].
Photon bunching noise also occurs while observing a light source. The light waves of the source are emitted independently but still interfere with each other. The consequence of this is that detected photons are not detected at randomly distributed times but arrive in bunches [20].

2.3. DESHIMA

In order to observe the high redshift galaxies we need a sensitive spectrometer that can sort the incoming signal by frequency. The Deep Spectroscopic High-redshift Mapper (DESHIMA) is a spectrometer that can be installed at ASTE. The goal of DESHIMA is to measure a wide spectrum of high redshift galaxies [11]. It is made up of Microwave Kinetic Inductance Detectors (MKIDs) which can sorts incoming light by frequency. The second version, DESHIMA 2.0, is in development and is planned to be be tested at ASTE in March 2022.

DESHIMA 2.0 has 347 frequency channels to measure over a range of 220 GHz to 440 GHz, making it possible to measure galaxies with various redshift. Each frequency channel consists of a microwave kinetic inductance detector (MKID) which combined measure the spectral signal that arrives at the telescope. The spectral resolution of DESHIMA 2.0 is $\frac{f}{\Delta f} = 500$, where Δf is the smallest difference in frequency that is distinguishable at a wavelength of f. The spectral resolution describes the ability of the chip to define small frequency intervals.

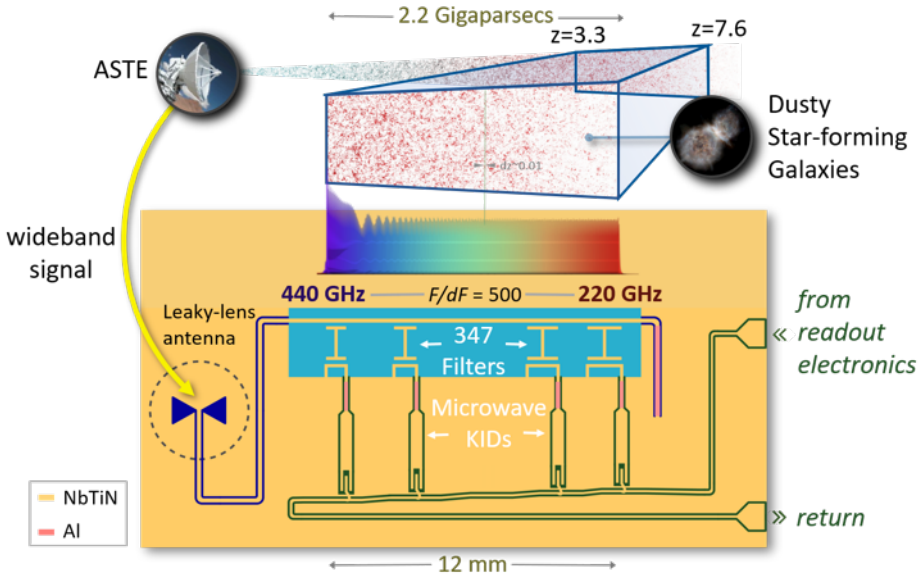

Figure 2.6: An illustration of the DESHIMA 2.0 chip. The light from the galaxies arives at the ASTE telescope. This signal is then sorted by frequency with the MKIDs in the DESHIMA chip.

When we look at the spectrum output of DESHIMA we have to take into account the frequency profile of the filters. They have a Lorentzian frequency profile, with the consequence that the line flux disseminates over multiple filters [7]. Therefore, if we simulate observations with DESHIMA we have to compare the outcome with a smoothed spectrum. In Figure 2.7 it is shown what a smoothed spectrum looks like compared to the original spectrum. The original spectrum is smoothed with a Lorentzian profile with the same width as the DESHIMA filters. For simplicity we omitted the possible absorption lines in Figure 2.7. For the same reason we only see the CII and a CO emission line.

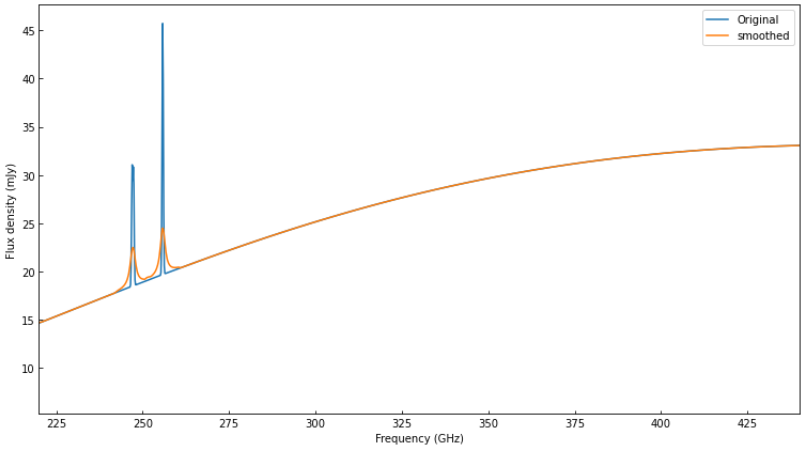

Figure 2.7: A simulation of an input spectrum where the absorption and several emission lines are omitted for simplicity. The frequency range is 220 - 440 GHz, the range of DESHIMA 2.0. The blue line is the spectrum as it is simulated to arrive at the telescope. The orange line indicates the spectrum smoothed with a Lorentzian profile to compensate for the frequency profile of the filters in DESHIMA 2.0

3

TiEMPO

Doing measurements with DESHIMA is costly and takes a lot of time. Therefore it is key to ascertain which sources can be measured and how long they need to be measured for in order to obtain a detection. In this chapter the Time-dependent End-to-end Model for Post-process Optimization, or TiEMPO is discussed, a model to predict the outcome of DESHIMA2.0 measurements. We dive into a previously existing problem that occurred when using multiple sky positions and explain how we resolved this problem.

3.1. Motivation

DESHIMA 2.0 is a relatively new instrument and has yet to be tested at the ASTE telescope. These tests are time consuming and costly. Additionally, there are various parameters that need to be determined, such as the measuring time. Deciding on the source of a measurement and the setup of the instrument has to be done in advance. In order to prepare the most promising observing strategy for DESHIMA 2.0 we want to do realistic simulations, which we then can use to decide the observation strategy. Ideally, we can also us the observations to prepare the analysis of the measurements. To this end the Time-dependent End-to-end Model for Post-process Optimization (TiEMPO) was developed. It is an open source python code which can be used to simulate measurements of DESHIMA 2.0. In Figure 3.1 you can find an overview of the components within TiEMPO.

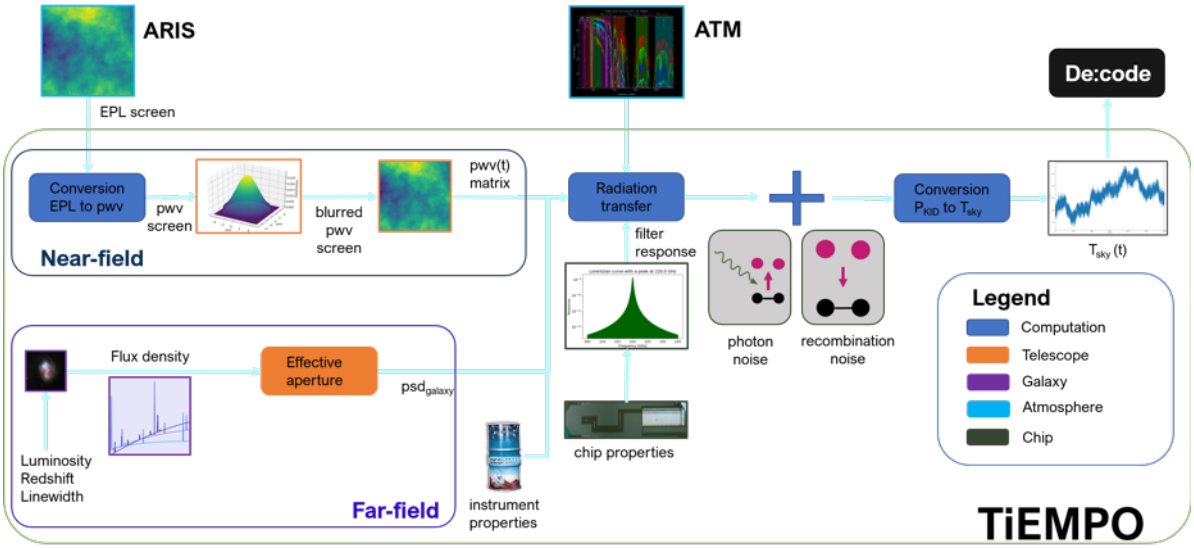

Figure 3.1: An overview of TiEMPO, where each component is shown with its input and output. The external models that TiEMPO uses are pictured as well.

3.2. Overview

Within this report we will focus on the aspects of the program which are relevant for the discussed research. This includes the galaxy spectrum generation in the far field, the atmosphere transmission as simulated from the precipitable water vapor (pwv) and the photon noise. The output of the model is discussed as well. A broader explanation on the workings of TiEMPO can be found in [6].

3.2.1. Noise sources

TiEMPO simulates different noise sources. It takes into account the photon noise, atmosphere transmission and instrument limitations.

ARIS
In order to simulate the effect of the atmosphere TiEMPO uses the Astronomical Radio Interferometer Simulator (ARIS) [21]. This tool outputs a two-dimensional map of the fluctuations in Extra Path Length (EPL) on a sky window. The rest of the model uses precipitable water vapor, so the EPL is converted to pwv.

Photon noise
The photon noise is added by drawing samples from the Poisson distribution.

3.2.2. Input spectrum

In Figure 3.1, the Far-field is where the galaxy spectrum is created and given as an input for the radiation transfer. In section 2.1 we saw that we measure a galaxy by its emission spectrum. Within TiEMPO it is possible to change the simulation model of the galaxy spectrum. The default to simulate the galaxy spectrum of the desired source is a model called galspec [22], which can be found on github. We used the spectrum shown in Figure 3.2 for this part of the project, where the spectrum is smoothed with a Lorentzian profile as explained in section 2.3.

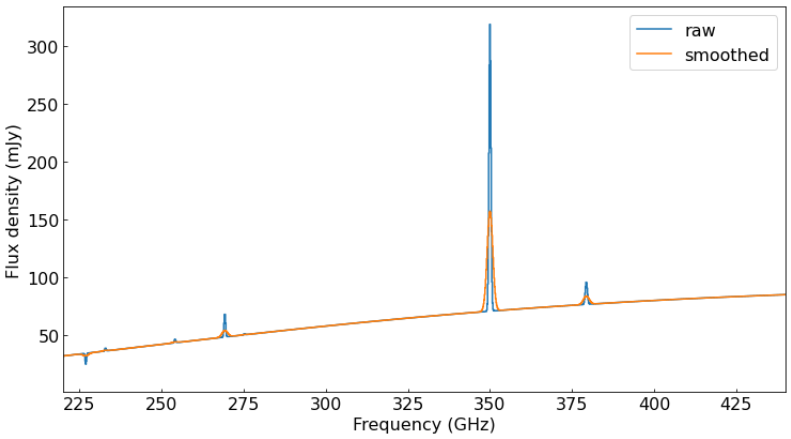

Figure 3.2: Simulated galaxy spectrum made using [22] with the frequency in GHz and the flux density in mJy. The blue line is the true simulated galaxy. The orange line is the same spectrum smoothed with a Lorentzian profile.

The spectrum has the specifications as shown in Table 3.1.

Parameter	Value
Minimum Frequency	220 [GHz]
Maximum Frequency	440 [GHz]
Redshift	4.43
Luminosity	$10^{13.7}$ $[L_{sol}]$
Frequency bins	1500
Full width half maximum	600 [km/s]

Table 3.1: These are the parameters needed to simulate the raw spectrum from Figure 3.2 with the python galspec package [22]. The minimum and maximum frequency are the frequencies at the observatory. They define the range of the measurements. The redshift determines the location of the peaks. The luminosity is the luminosity of the galaxy. The frequency bins are the number of linearly spaced frequency bins at which the spectrum is evaluated. The FWHM determines the width of the emission lines.

When simulating a galaxy spectrum for TiEMPO the height and width of the emission lines are key. We rely on the correctness of them to tell whether a galaxy is detectable.

3.2.3. Output data

TiEMPO outputs the simulation data in T_{sky} and power. The data is per time step per frequency channel. Calculating the flux density F_f from T_{sky} can be done using equation 3.1

$$F_f(T_{sky}) = \frac{2\Omega_A}{\lambda^2 \eta_{atm}} \frac{hf}{e^{\frac{hf}{k_B T_{sky}}} - 1} \tag{3.1}$$

Where Ω_A is the beam solid angle in sr, η_{atm} the atmosphere transmission, λ the wavelength in m and f the frequency in Hz. k_B is the Boltzmann constant and h the Planck constant.

3.3. Development

Since TiEMPO is fairly new some features haven't been thoroughly tested and developed, and still need to be updated. One of the problems which had to be solved was simulating measurements of 6 sky positions at once, in order to apply AB chopping in multiple directions. As explained in chapter 2.2.1, we need to measure two positions in order to apply AB chopping. During measurements the positions can be under an arbitrary angle with the wind. This angle is important since it decides what the atmosphere difference between the positions is. Taking an arbitrary angle is not possible within TiEMPO, but it is possible to take positions perpendicular to or parallel with the wind. Figure 3.3 indicates which positions can be simulated. Being able to take 6 different positions gives more options with regard to simulations and the AB chopping during post processing.

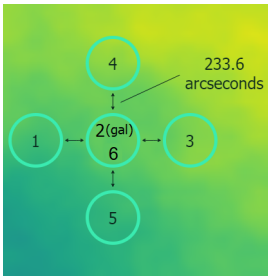

Figure 3.3: The 6 sky positions that can be simulated during a TiEMPO simulation. If we indicate from the centre position 2 and 6 then position 1 and 3 are in line with the wind and position 4 and 5 perpendicular to the wind. The wind is simulated to come from the left.

The six sky positions are, (1) left, (2) centre with a galaxy, (3) right, (4) Top, (5) bottom and (6) centre without a galaxy. Top (4) and bottom (5) are the positions perpendicular to the wind and left (1) and right (3) in line with the wind compared to the centre position. Simulating the four left, right and both centre positions has been tested and works, but adding the top and bottom position caused problems. The simulations were not correct and it seemed like values of the positions were swapped during the calculations. Therefore the code had to be corrected.

3.3.1. Problem sketch

After subtracting a simulation of one of the positions from the on position you expect to be left with the galaxy and some influence from the noise sources. For good values of the atmosphere transmittance every position simulation should follow the continuum of the simulated galaxy after the atmosphere emission is removed. With the 4 sky positions left, centre on, centre off and right this was indeed the case, but as you can see in Figure 3.4 something went wrong when 6 sky positions are used.

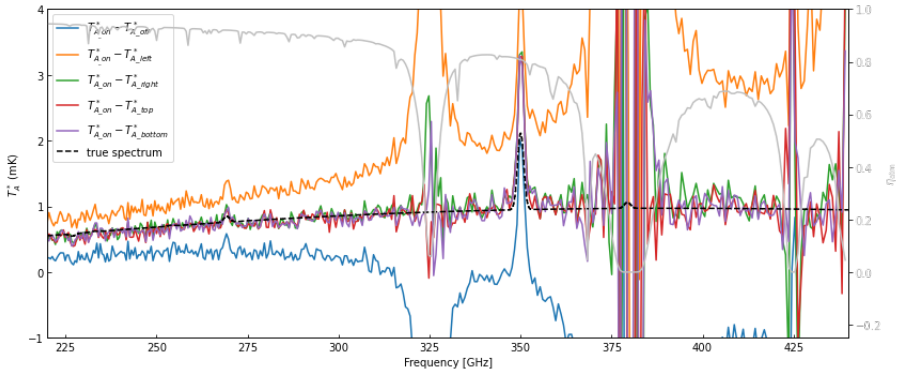

Figure 3.4: A 1h TiEMPO simulation with the antenna temperature T_A^* in mK versus the frequency in GHz where 6 sky positions are used. The lines indicate the difference between the simulation of the position with the galaxy minus a position without a galaxy, corrected for the atmosphere transmission. The CII peak is visible at 350GHz. The values for the off and left position behave unexpectedly. The rest of the data seems to be in in line with the true input spectrum.

In Figure 3.4 the lines of the right, top and bottom position is as we would expect, but the off and left position are incorrect. In order to find the place in the code where the problem occurs we have to work systematically. First we have to map out the problem so we know what to look for.

3.3.2. Approach

In order to simplify the problem we decided to turn off the photon noise and run TiEMPO for a shorter time. When a simulation is run, the smoothed spectrum should show up at a fairly small integration time, since the CII emission peak is high compared to the expected noise. This is only the case because we omit part of the noise, the emission line is high enough and the line doesn't fall in the worst atmosphere transmission intervals. With the photon noise removed we had to check if the problem was still occurring. In image 3.5 we can see that it indeed does, and that two positions behave unexpectedly.

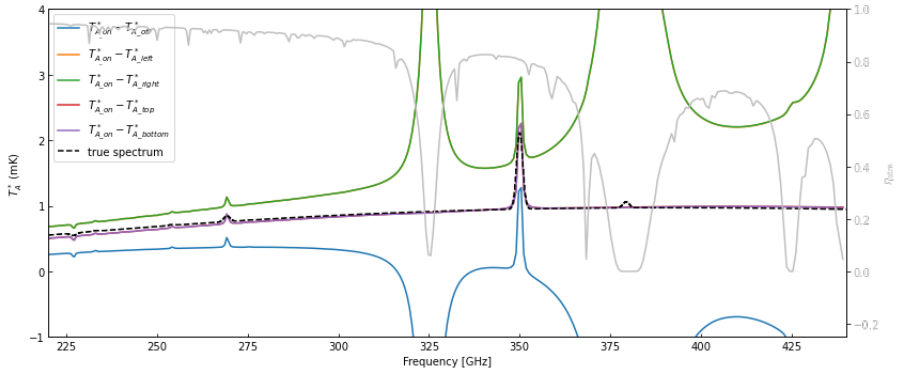

Figure 3.5: A 50 second TiEMPO simulation of the simulated antenna temperature T_A^* in mK against the frequency in GHz. The lines indicate the difference between the simulation of the position with the galaxy minus a position without a galaxy. The photon noise is turned off in this simulation. The green and orange line overlap, as well as the purple and red line.

In Figure 3.5 the atmosphere interference is evident, and at 350 GHz the CII emission line is also visible. Since the CII line is visible in all subtractions we can conclude that the position containing the galaxy is not swapped with another position. This position is calculated separately at multiple locations within the code which could explain why this position is different.

From these images and the fact that the problem doesn't happen during a simulation with 4 positions at the same x-coordinates, the idea came to be that some beams were swapped during the calculation based on the height of the values for each position. For this reason we tested the order of the beams at the beginning and at the end of the calculation. A higher pwv value for a position at the beginning of the calculations should result in a higher power value at the end. During the tests we saw that this was not the case, therefore positions had to be swapped in the calculations from pwv to power. The next step was to check the values in between

calculations, starting with values in the middle to exclude big parts of the code at once. With this technique the correct line of code was eventually found.

3.3.3. Solution

The solution to this problem was quite simple in the end. A for loop needed to be added in order to prevent the interp2D function from SciPy [23] from ordering the values of the different positions in size. These changes have been made and are included in the current version of the program. The six sky positions can now be used for future simulations. In Figure 3.6 is shown what the output of a correct simulation with 6 sky positions should look like.

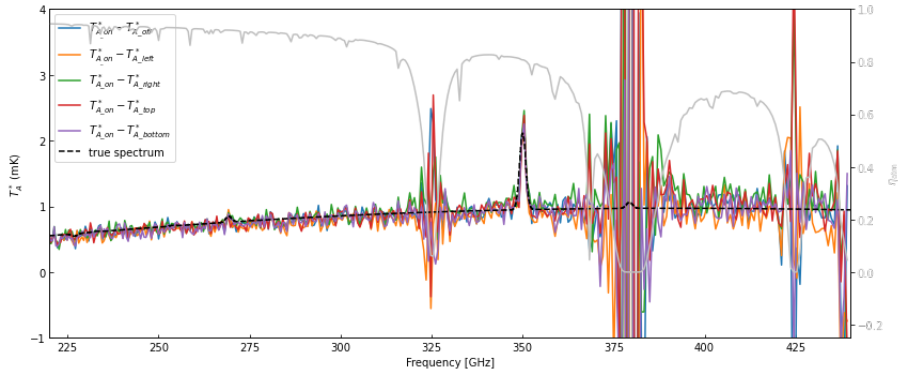

Figure 3.6: An 1h TiEMPO simulation of the simulated antenna temperature T^*_A in mK against the frequency in GHz. The lines indicate the difference between the simulation of the position with the galaxy minus a position without a galaxy.

4

Analysis of a full 8 hour Simulation

In this chapter we analyse the TiEMPO simulation of the dusty starburst galaxy HFLS3. This galaxy is a good candidate to see where the limits of DESHIMA 2.0 lie, because it is a galaxy with a faint CII emission line. We look at the emission spectrum and input spectrum for TiEMPO. Thereafter we present a full TiEMPO simulation and discuss the results.

4.1. HFLS3

In order to thoroughly test TiEMPO we want to do a long simulation of a high redshift galaxy. We chose HFLS3, a dust-obscured massive maximum-starburst galaxy at a redshift of 6.34 [2]. This galaxy is already well documented, and has a well-sampled spectrum including the CII emission line. The spectrum as measured in the paper can be seen in Figure 4.1. The CII line can be found at a frequency of 1900 GHz.

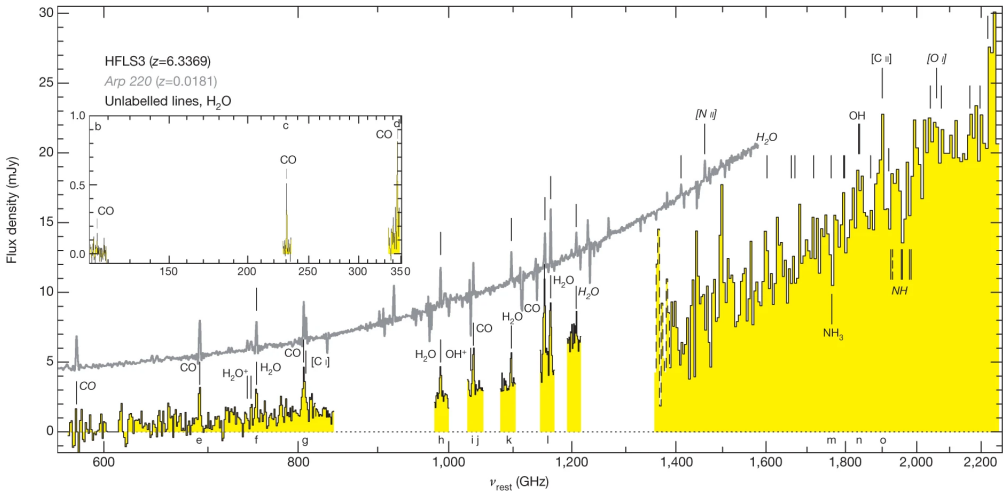

Figure 4.1: Emission spectrum of the dusty starburst galaxy HFLS3 from [2] with the flux density in mJy versus the rest frequency in GHz.

The galaxy has the specifications as shown in Table 4.1.

Parameter	Value
Redshift (z)	6.34
Dust temperature (T_{dust})	56 [K]
Far infrared luminosity (L_{FIR})	$2.86 \cdot 10^{13}$ [L_{sol}]
Beta (β)	1.92
Full witdh half maximum ($FWHM$) of the CII line	470 [km s^{-1}]

Table 4.1: These are the parameters needed from [2] in order to run a TiEMPO simulation.

The β corresponds to the slope of the spectrum and is an indicator for the emissivity of a galaxy. The dust temperature T_{dust} is derived from spectral energy distribution fitting as described in [2]. The $FWHM$ is solely for the CII emission line. In this report the other emission lines are not taken into account. While simulating the emission spectrum the other lines which are present do however get the same $FWHM$ as the CII line, while they should be narrower.

At a redshift of $z = 6.34$ we expect to find the CII emission line at a frequency of 259 GHz. With this redshift we look back at the universe to when it was just 880 million years old, which is $\frac{1}{16}^{th}$ of its present age [2].

4.1.1. Difference in spectrum simulations

As mentioned in section 2.1.2 there are multiple models to predict the height of the CII emission lines. So far the simulations made with TiEMPO have adopted emission spectra based on models from Bonato et al. [13]. HFLS3 is however much more CII deficient than predicted in the Bonato models. In Figure 4.2 we can see HFLS3 in the bottom right corner. It has a high Star Forming Rate (SFR) but a low ratio of CII luminosity vs total luminosity $L_{CII}/L_{TIR} \approx 0.025\%$. This corresponds to a ratio of $\frac{L_{CII}}{L_{FIR}} = 5e-4$. Bonato models predict that $\frac{L_{CII}}{L_{FIR}} = 1.8e-3$.

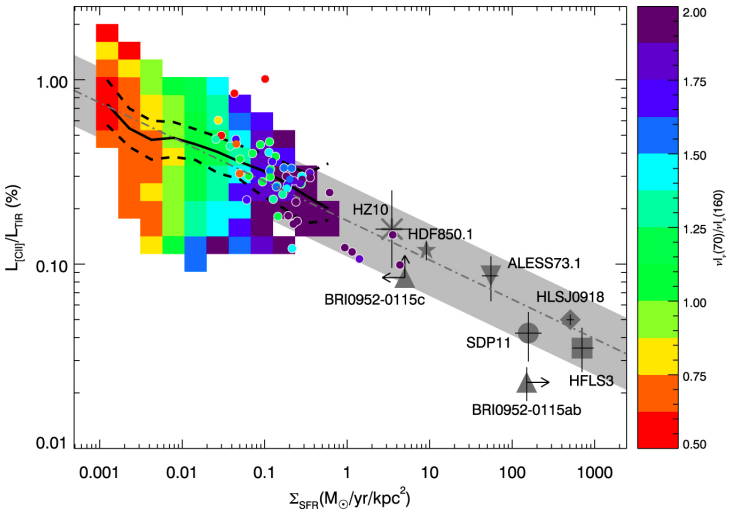

Figure 4.2: The trend in CII deficit with star forming rate density ($\sum_{SFR}$). The filled circles are well-resolved nearby luminous infrared galaxies. The gray points are high-redshift sources with resolved CII emission lines. The galaxy HFLS3 can be found in the bottom right corner. This image is from [2].

The consequence of this is that the standard simulation of the galaxy needs to be adapted in order to correctly predict the height of the CII emission line. Figure 4.3 shows the comparison between the Bonato models and a model based on [14], specifically created for HFLS3 by M. Rybak.

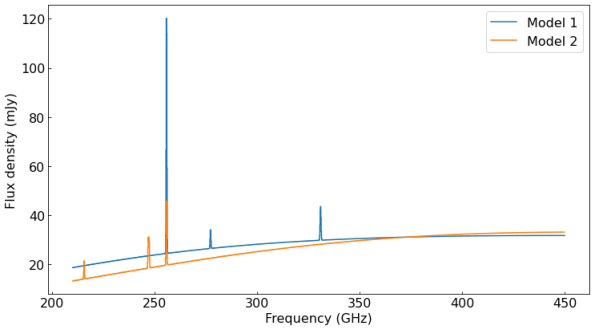

(a) Comparison over the full frequency range of 220 – 440 GHz of DESHIMA2.0.

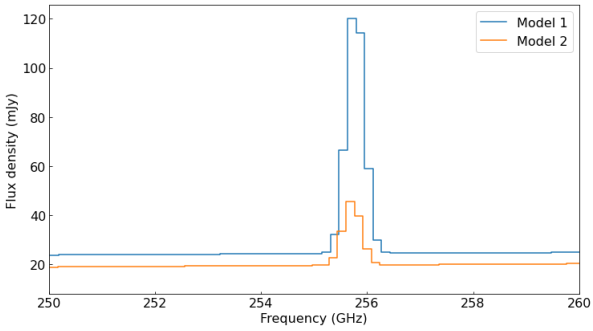

(b) Comparison over a frequency range of 250–260 GHz zoomed in around the CII emission line.

Figure 4.3: Simulation of the emission spectrum arriving on Earth in flux density in mJy versus the frequency in GHz of the dusty starburst galaxy HFLS3 based on two different models. Model 1 is the Bonato model from [13] and model 2 is based on [14].

The lines at 259 GHz are the predictions for the CII line of both models.

4.1.2. Lorentzian filter

In section 2.3 we explained we need to smooth the input spectrum with a Lorentzian profile to accommodate for the MKIDs in our spectrometer. The comparison between the raw and smoothed spectrum can be found in Figure 4.4.

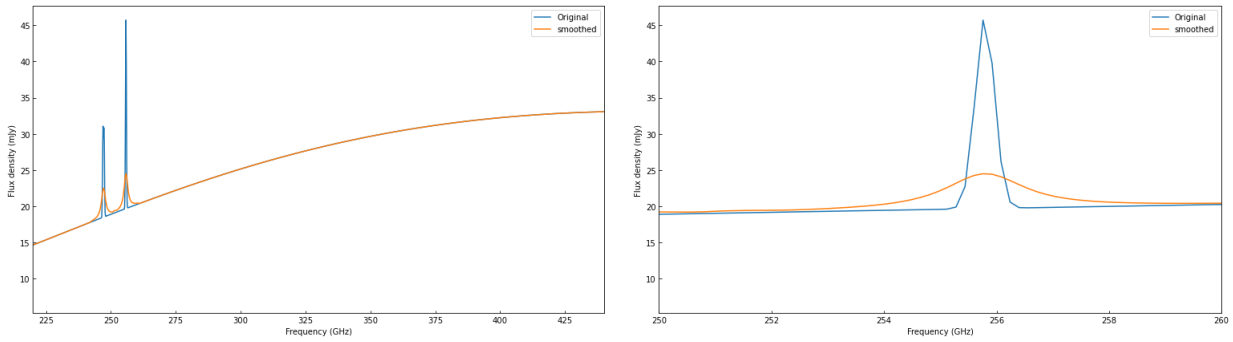

(a) Comparison over the full frequency range of 220 – 440 GHz of DESHIMA2.0.

(b) Comparison over a frequency range of 250−260 GHz zoomed in around the CII emission line.

Figure 4.4: Simulation of the observed emission spectrum in flux density in mJy versus the frequency in GHz of the dusty starburst galaxy HFLS3. The spectrum is compared to a smoothed simulation. The smoothed spectrum can be compared to the output of a TiEMPO simulation.

It can be seen that the height of the peak decreases significantly when the spectrum is smoothed.

4.2. Atmosphere predictions

To correct the data for the atmosphere transmission this transmission needs to be simulated. To do so we need an average precipitable water vapor (pwv) value, close to the values we expect during measurements. In Figure 4.5 the atmosphere transmission is simulated for average pwv values of 1.0 mm and 0.5 mm. It is clear to see that the transmission is better for the lower pwv value.

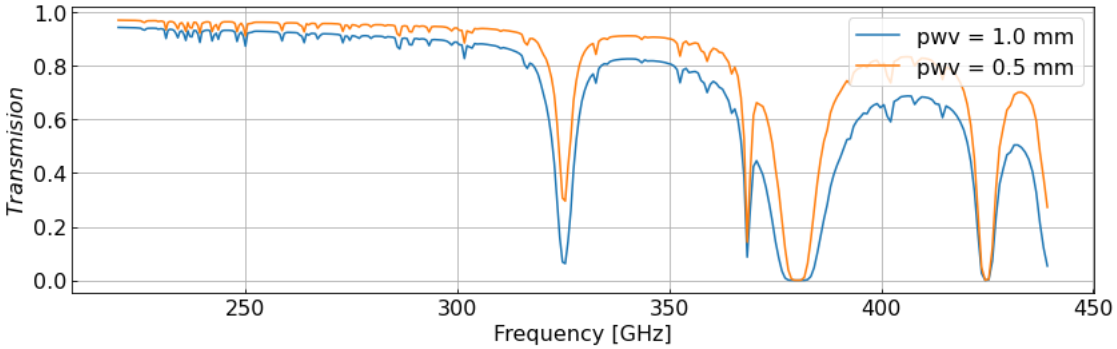

Figure 4.5: The transmission of the atmosphere against the frequency in GHz. The transmission is calculated for a pwv value of 1.0 mm and 0.5 mm.

Since the atmosphere fluctuates, as simulated with ARIS, the atmosphere transmission in Figure 4.5 is a approximation of the transmission during the complete measurement, and will be used during the calculations as the transmission. The fluctuations will result in atmosphere noise.

4.3. SNR

To determine if a emission line is detected the general rule is that the detected peak has to be 5 times the standard deviation of the signal. You can also say that the Signal to Noise Ratio (SNR) has to be greater than 5. For our measurement we expect the standard deviation σ to decrease with integration time according to the

relation $\sigma \propto \tau^{-0.5}$ [24]. For this reason it is beneficial to increase the integration time. The σ is also dependent on the atmosphere, so a lower pwv value would result in a lower σ and generally a higher SNR.

In order to find the σ of our simulations we have to do some calculations. First, the continuum has to be taken out of the simulation. To accomplish this a line is fitted trough the data points. Since the emission spectrum in the frequency range above 310 GHz is very poor because of the atmosphere absorption we don't take into account this part of the data. So we fit a line trough the data points between 220 – 310 GHz. After subtracting this line from the simulation we only have the noise and emission lines left. Then the standard deviation σ can be calculated as in equation 4.1.

$$\sigma = \sqrt{\frac{\sum(x_i - \mu)}{N}} \tag{4.1}$$

with N the number of data points, x_i each measurement point and μ the mean of the data points. For this calculation we use the frequency range of 220 – 245 GHz and 260 – 310 GHz, since the emission lines can be seen within the 245 – 260 GHz frequency range. During a measurement with DESHIMA 2.0 these ranges may be more difficult to predict. In this case it would be wise to try multiple ranges.

4.4. Expectations

In order to predict whether a galaxy can be measured we can use the deshima-sensitivity python package on github [25] which allows us to determine the observation sensitivity of DESHIMA 2.0. In Figure 4.6 two predictions are made, in Figure 4.6a the observation time is 8 hours, and in 4.6b the observation time is 16 hours.

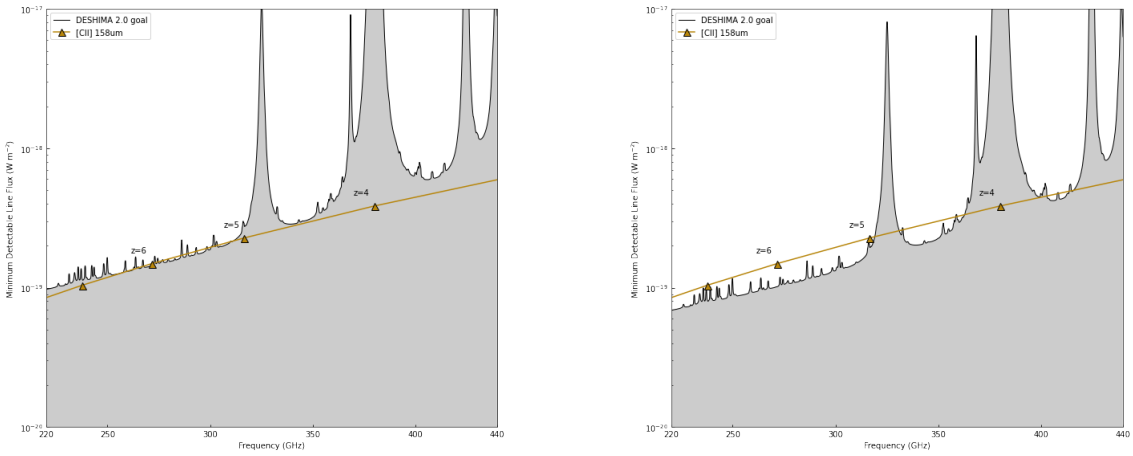

(a) Expectation of the CII line flux after 8 hours.

(b) Expectation of the CII line flux after 16 hours.

Figure 4.6: An expectation of the sensitivity of DESHIMA 2.0 for a simulation of the galaxy HFLS3 with an average pwv value of 1.0 mm. The yellow line is the predicted line flux for the CII emission line and the grey line the goal of minimal detectable line flux for DESHIMA 2.0.

From Figure 4.6a we see that with an 8 hour simulation with a pwv value of 1.0 mm we are at the edge of the DESHIMA 2.0 sensitivity. For an 16 hour simulation with the same specifications we should be able to measure HFLS3, since it has a redshift of 6.34.

The same comparison can be made for two simulations with the same input variables except for different pwv values.

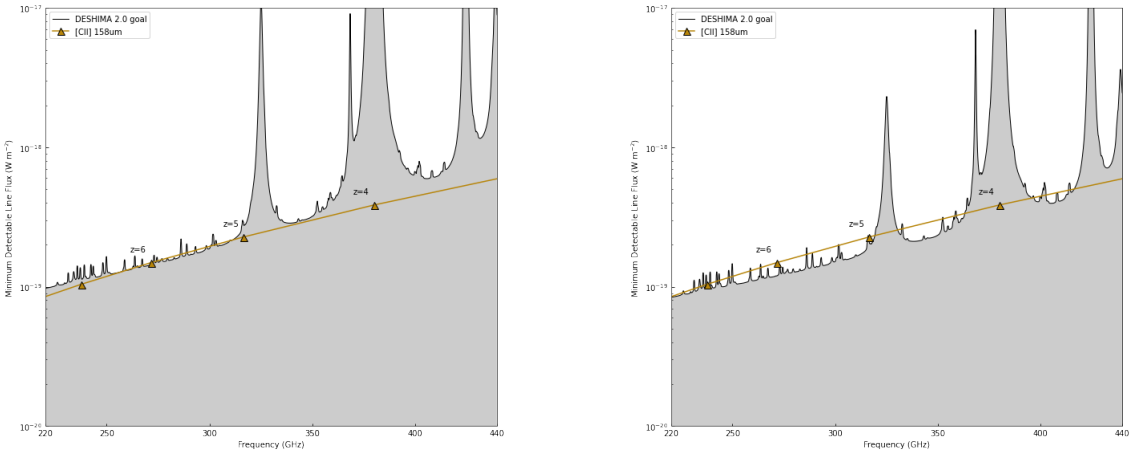

(a) Expectation of the CII line with pwv = 1.0 mm.

(b) Expectation of the CII line with pwv = 0.5 mm.

Figure 4.7: An expectation of the sensitivity of DESHIMA 2.0 for a simulation of the galaxy HFLS3 with an observation time of 8 hours. The yellow line is the predicted line flux for the CII emission line and the grey line the goal of minimal detectable line flux for DESHIMA 2.0.

The simulation with a pwv value of 0.5 seems to detectable after 8 hours if you look at Figure 4.7b.

4.4.1. Data Loss

Due to the earlier explained AB chopping we lose a lot of simulation data in order to get a realistic result. First, since the data output is in different files we need to make sure the files are the right size to apply AB chopping. The files need to be a multiple of 16 time steps, since we switch positions every 8 time steps. The data we lose with this is small, since we have to delete at most 15 time steps per file. This accounts to roughly 0.1 second, and we have 16 files so at most 1.6 seconds. We then remove half of the data for each position, the time where in a real measurement the telescope would be pointed at the other spot. This data loss is taken into account during the calculations of the observation sensitivity of DESHIMA 2.0 as shown in Figure 4.6 and 4.7.

4.5. TiEMPO simulation

A full 8 hour simulation of the HFLS3 spectrum can be found in Figure 4.8. For this simulation we used the smoothed input spectrum as shown in Figure 4.4 and a pwv value of 1.0 mm.

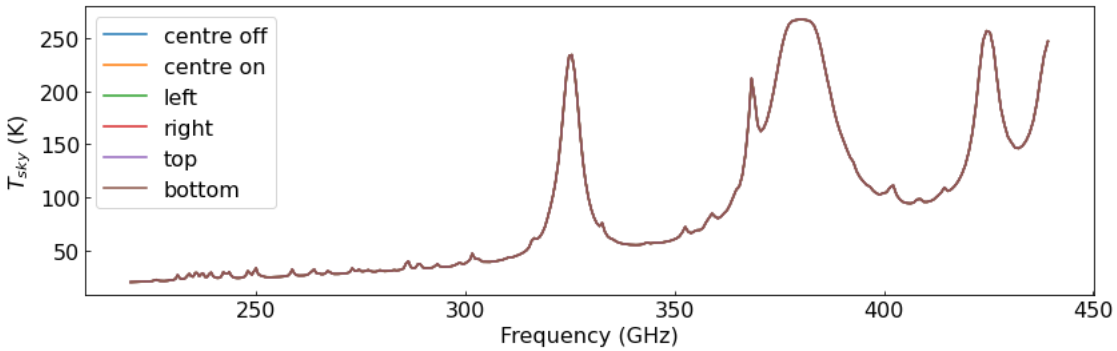

Figure 4.8: The simulated T_{sky} data in K against the frequency in GHz of the galaxy HFLS3 after 8 hours for 6 different sky positions. The six positions overlap because the data is not yet corrected for the atmosphere transmission.

From this plot we can't conclude much besides the fact that for all positions the atmosphere emission determines the shape of the T_{sky} data. This is expected since the galaxy signal is much fainter than the signal from the atmosphere. In order to find the galaxy signal we subtract the off position from the on position, after which the data is corrected for the atmosphere transmission, as simulated in section 4.2. The calculation is done according to equation 4.2.

$$T_A^* = \frac{T_{sky\_on} - T_{sky\_off}}{\eta_{atm}} \tag{4.2}$$

To compare the simulation with the original paper these temperatures are then converted to flux density according to equation 3.1.

4.5.1. Comparison over time

The result of the simulation after these calculations can be found in Figure 4.9.

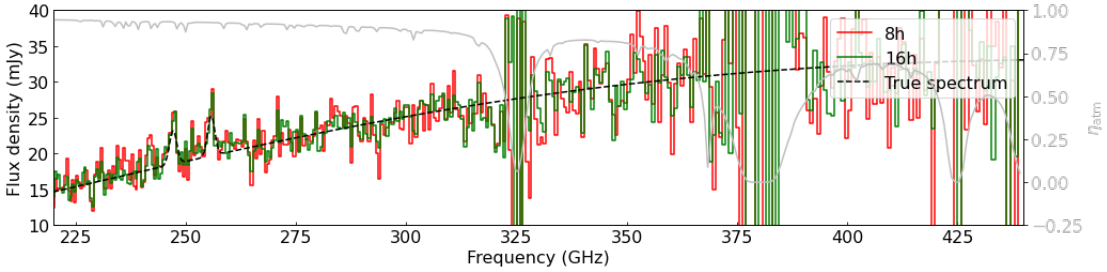

(a) Frequency range of 220 – 440 GHz. The frequency is the observed frequency.

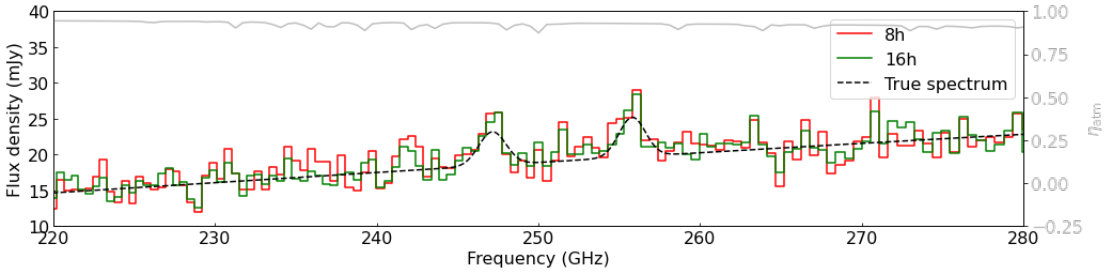

(b) Frequency range of 220 – 280 GHz. The frequency is the observed frequency.

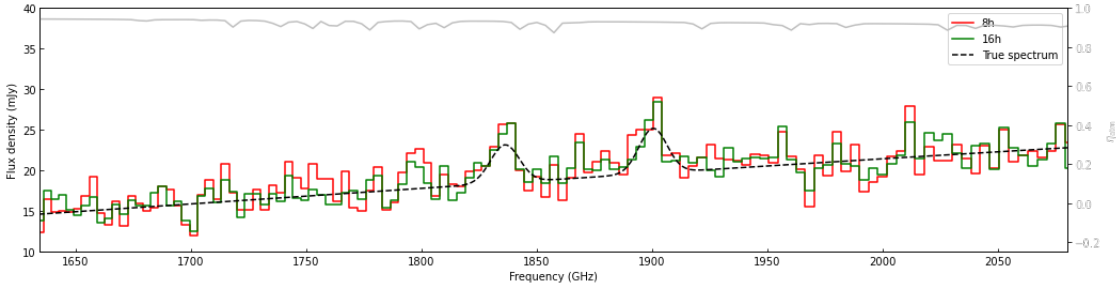

(c) Frequency range of 1630 – 2080 GHz. Here the frequency is converted to the rest frequency by multiplying the observed frequency with $(1+z)$.

Figure 4.9: TiEMPO simulation of HFLS3 with the flux density in mJy vs the frequency in GHz. In the plot the red line is a simulation of 8 hours and the green line a simulation of 16 hours. For both simulations the pwv value is 1.0 mm. The black dashed line is the expected spectrum of HFLS3, smoothed to account for the resolving power of the spectrometer. The flux density is obtained by subtracting the centre off data from the centre on data, and corrected for the atmosphere transmission.

In Figure 4.9b the CII seems to be visible at 259 GHz. Figure 4.9c can be compared to Figure 4.1. The CII lines have the same frequency. The height of the CII line is a bit higher in our simulation. To determine if the galaxy is indeed detected the signal to noise ration is calculated.

The value of σ over time for a 16h simulation where pwv = 1.0 mm are shown in Figure 4.10

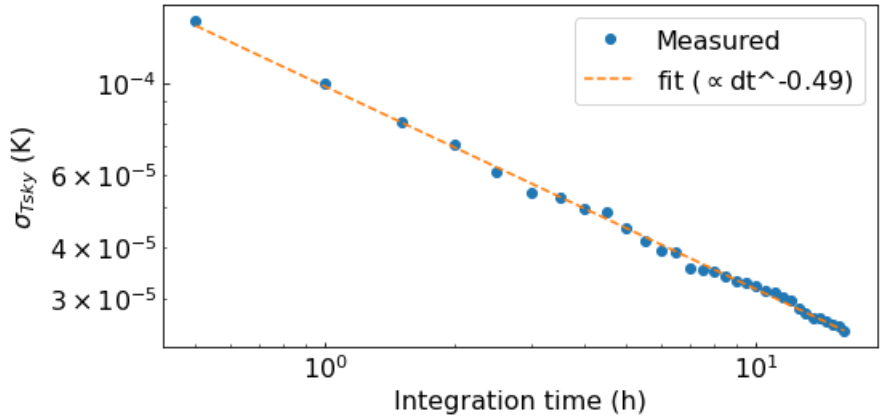

Figure 4.10: The σ vs the integration time of an 16h TiEMPO simulation with a pwv value of 1.0mm. The axis are in log scale.

The fitted relation between σ and integration time agrees with the expected relation of $\sigma = \propto \tau^{-0.5}$.

For the 16 hour simulation we have calculated the Signal to Noise Ratio (SNR) over time. The values can be found in Figure 4.11.

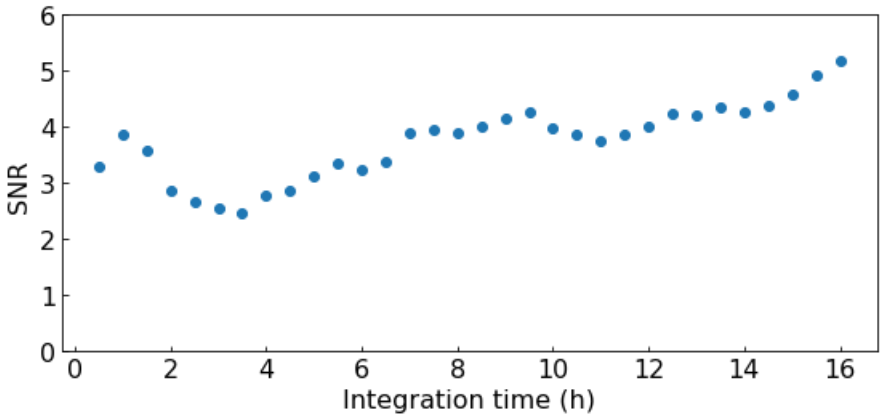

Figure 4.11: The SNR vs the integration time of an 16h TiEMPO simulation with a pwv value of 1.0.

After 16 hours of observation the SNR is 5.1. This is just above the 5 σ limit, and we can therefore say that the galaxy can be detected after 16 hours of observation.

4.5.2. Comparison with different pwv values

The average pwv value during the measurements influences the observation time necessary to observe the galaxy. Therefore, we compared two 8 hour simulations with different pwv values. One simulation has a pwv value of 1.0 mm and the other has a pwv value of 0.5 mm. The results can be found in Figure 4.12.

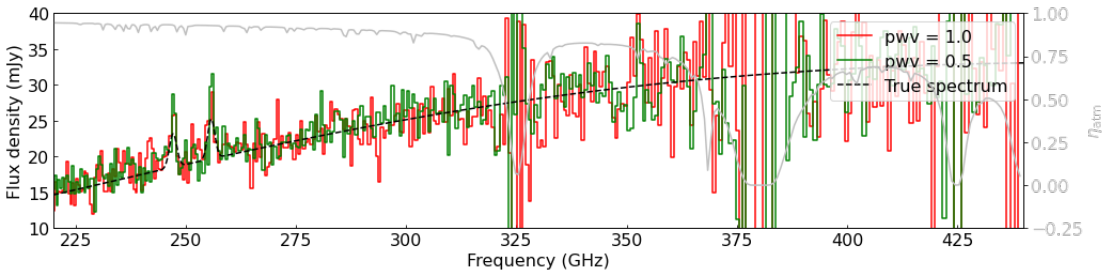

(a) Frequency range of 220 – 440 GHz. The frequency is the observed frequency.

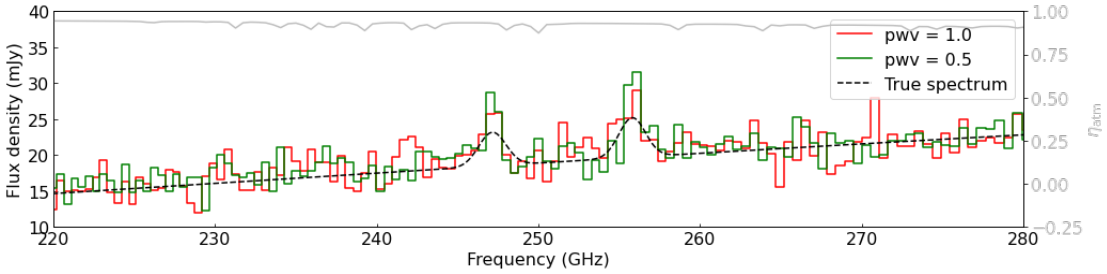

(b) Frequency range of 220 – 280 GHz. The frequency is the observed frequency.

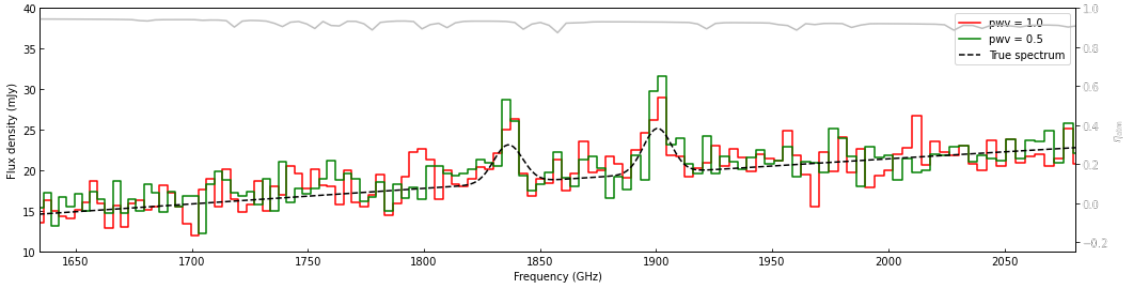

(c) Frequency range of 1630 – 2080 GHz. Here the frequency is converted to the rest frequency by multiplying the observed frequency with $(1+z)$.

Figure 4.12: TiEMPO simulation of HFLS3 with the flux density in mJy vs the frequency in GHz. In the plot the red line is a simulation with a pwv value of 1.0 mm and the green line a simulation with a pwv value of 0.5 mm. For both simulations the observation time is 8 hours. The black dashed line is the expected spectrum of HFLS3, smoothed to account for the resolving power of the spectrometer. The flux density is obtained by subtracting the centre off data from the centre on data, and corrected for the atmosphere transmission.

For these simulations the SNR is calculated. After 8 hours of observation, the SNR is 3.9 for a pwv value of 1.0 mm and 6.0 for a pwv value of 0.5mm. This means that we don't have an observation for the higher pwv value, but the lower value does give a significant observation after 8 hours. The pwv value influences the necessary observation time significantly.

5

Conclusions and future prospects

5.1. Conclusions

In this report, a solution was introduced to improve the Time-dependent End-to-end Model for Post-process Optimization (TiEMPO). It is now possible to use 6 different sky positions while simulating DESHIMA 2.0 measurements with TiEMPO. This accommodates the simulation of different scenario's for wind direction, and can be used in future simulations.

The main focus of this report however, is the analysis of a TiEMPO simulation of the dusty starburst galaxy HFLS3. In order to get a realistic simulation the input spectrum had to be simulated beforehand. While comparing different simulations of the emission spectrum of HFLS3 we came to the conclusion that the default options in TiEMPO are not always applicable, especially for high redshift galaxies. Since these are the main observation goals for DESHIMA 2.0 we used a different model to simulate our spectrum.

With this spectrum we did several simulations, with different observation times and pwv values. We say that a emission line is detected if the SNR is greater than 5. The calculated SNR of a 16 hour observation with a pwv value of 1.0 mm is 5.2, which shows that HFLS3 can be detected. Lowering the pwv value to 0.5 mm improves the SNR significantly for shorter observation times. The SNR after 8 hours of observation is 3.9 for a pwv value of 1.0 mm and 6.0 for a pwv value of 0.5mm. During the on site DESHIMA measurements, the atmosphere conditions will have a big influence on the observation time that is needed to detect a galaxy.

5.2. Future Prospects

While solving the problem within TiEMPO regarding the 6 sky positions there was another problem discovered. Currently the 4 positions left, centre on, right and centre off are all set at the same position at the start of the simulation. Only at the end do the positions get translated to the correct x-coordinate. With the introduced solution for adding the top and bottom sky position it should be possible to give the positions the correct coordinate from the beginning. The code can be simplified by changing the way the horizontal positions are added to the code. Why this gives different results to the current implementation can be looked into further.

Furthermore, as described in the report we need to be careful while simulating the input galaxy in TiEMPO. It is essential to accurately predict the spectrum and emission lines as to make a realistic simulation. To accommodate for this, TiEMPO could be further developed to be able to take different models as input for galaxy simulations.

For the simulation we analysed in this report the galaxy spectrum that was given as input was known. Knowing where the emission lines are played a part in the calculation of the SNR. During on site observations with DESHIMA 2.0 this is generally not the case, it would be interesting to analyse a TiEMPO simulation of which the input parameters are unknown. This could have an influence on the way the σ and SNR are calculated.

For the on site observation strategy of DESHIMA 2.0 a database of TiEMPO simulations for different galaxies would be of added value. For this a list of interesting galaxies would have to be made, including their specifications as far as they are known. The database could also include hypothetical galaxies which are perhaps not yet detected but have properties we could expect to measure during observations.

Bibliography

[1] Star factory in the early universe challenges galaxy evolution theory. https://www.esa.int/Science_Exploration/Space_Science/Herschel/Star_factory_in_the_early_Universe_challenges_galaxy_evolution_theory.

[2] Dominik A. Riechers, C. M. Bradford, D. L. Clements, C. D. Dowell, I. Pérez-Fournon, R. J. Ivison, C. Bridge, A. Conley, Hai Fu, J. D. Vieira, J. Wardlow, J. Calanog, A. Cooray, P. Hurley, R. Neri, J. Kamenetzky, J. E. Aguirre, B. Altieri, V. Arumugam, D. J. Benford, M. Béthermin, J. Bock, D. Burgarella, A. Cabrera-Lavers, S. C. Chapman, P. Cox, J. S. Dunlop, L. Earle, D. Farrah, P. Ferrero, A. Franceschini, R. Gavazzi, J. Glenn, E. A. Gonzalez Solares, M. A. Gurwell, M. Halpern, E. Hatziminaoglou, A. Hyde, E. Ibar, A. Kovács, M. Krips, R. E. Lupu, P. R. Maloney, P. Martinez-Navajas, H. Matsuhara, E. J. Murphy, B. J. Naylor, H. T. Nguyen, S. J. Oliver, A. Omont, M. J. Page, G. Petitpas, N. Rangwala, I. G. Roseboom, D. Scott, A. J. Smith, J. G. Staguhn, A. Streblyanska, A. P. Thomson, I. Valtchanov, M. Viero, L. Wang, M. Zemcov, and J. Zmuidzinas. A dust-obscured massive maximum-starburst galaxy at a redshift of 6.34. *Nature*, 496(7445):329–333, 2013.

[3] Christopher J. Conselice, Aaron Wilkinson, Kenneth Duncan, and Alice Mortlock. The evolution of galaxy number density at z < 8 and its implications. *The Astrophysical Journal*, 830(2):83, oct 2016.

[4] Information@eso.org. The formation of stars, 2011. https://esahubble.org/science/formation_of_stars/.

[5] C. Kulesa. Terahertz spectroscopy for astronomy: From comets to cosmology. *IEEE Transactions on Terahertz Science and Technology*, 1:232–240, 2011.

[6] E. Huijten. Tiempo: Time-dependent end-to-end model for post-process optimiza- tion of the deshima spectrometer. *Bachelor's thesis, Delft University of Technology*, 2020.

[7] Esmee Huijten, Yannick Roelvink, Stefanie A. Brackenhoff, Akio Taniguchi, Tom Bakx, Kaushal B. Marthi, Stan Zaalberg, Jochem J. A. Baselmans, Kah Wuy Chin, Robert Huiting, and et al. Tiempo: Open-source time-dependent end-to-end model for simulating ground-based submillimeter astronomical observations. *Millimeter, Submillimeter, and Far-Infrared Detectors and Instrumentation for Astronomy X*, Dec 2020.

[8] Glossary, 2019. https://hubblesite.org/glossary.html#h3-CK-c9341de0-583b-43c7-81f6-8e9d528c521a.

[9] Andy Anderson, 2019. https://commons.wikimedia.org/w/index.php?curid=84111964.

[10] P. A. R. Ade, N. Aghanim, M. Arnaud, M. Ashdown, J. Aumont, C. Baccigalupi, A. J. Banday, R. B. Barreiro, J. G. Bartlett, and et al. Planck 2015 results. *Astronomy & Astrophysics*, 594:A13, Sep 2016.

[11] Akira Endo, Kenichi Karatsu, Yoichi Tamura, Tai Oshima, Akio Taniguchi, Tatsuya Takekoshi, Shin'ichiro Asayama, Tom J. L. C. Bakx, Sjoerd Bosma, Juan Bueno, Kah Wuy Chin, Yasunori Fujii, Kazuyuki Fujita, Robert Huiting, Soh Ikarashi, Tsuyoshi Ishida, Shun Ishii, Ryohei Kawabe, Teun M. Klapwijk, Kotaro Kohno, Akira Kouchi, Nuria Llombart, Jun Maekawa, Vignesh Murugesan, Shunichi Nakatsubo, Masato Naruse, Kazushige Ohtawara, Alejandro Pascual Laguna, Junya Suzuki, Koyo Suzuki, David J. Thoen, Takashi Tsukagoshi, Tetsutaro Ueda, Pieter J. de Visser, Paul P. van der Werf, Stephen J. C. Yates, Yuki Yoshimura, Ozan Yurduseven, and Jochem J. A. Baselmans. First light demonstration of the integrated superconducting spectrometer. *Nature Astronomy*, 3(11):989–996, 2019.

[12] Lagache, G., Cousin, M., and Chatzikos, M. The [cii] 158 ne emission in high-redshift galaxies. *A&A*, 609:A130, 2018.

[13] M. Bonato, M. Negrello, Z.-Y. Cai, G. De Zotti, A. Bressan, A. Lapi, C. Gruppioni, L. Spinoglio, and L. Danese. Exploring the early dust-obscured phase of galaxy formation with blind mid-/far-infrared spectroscopic surveys. *Monthly Notices of the Royal Astronomical Society*, 438(3):2547–2564, 01 2014.

[14] J. D. T. Smith, Kevin Croxall, Bruce Draine, Ilse De Looze, Karin Sandstrom, Lee Armus, Pedro Beirão, Alberto Bolatto, Mederic Boquien, Bernhard Brandl, and et al. The spatially resolved [cii] cooling line deficit in galaxies. *The Astrophysical Journal*, 834(1):5, Dec 2016.

[15] Mini Physics, Remedy, Anonymous, Joe, Max Radford, and Francis Riemensperger. The electromagnetic spectrum, May 2016.

[16] Caitlin M. Casey, Desika Narayanan, and Asantha Cooray. Dusty star-forming galaxies at high redshift. *Physics Reports*, 541(2):45–161, Aug 2014.

[17] V. Asboth, A. Conley, J. Sayers, M. Béthermin, S. C. Chapman, D. L. Clements, A. Cooray, H. Dannerbauer, D. Farrah, J. Glenn, S. R. Golwala, M. Halpern, E. Ibar, R. J. Ivison, P. R. Maloney, R. Marques-Chaves, P. I. Martinez-Navajas, S. J. Oliver, I. Pérez-Fournon, D. A. Riechers, M. Rowan-Robinson, Douglas Scott, S. R. Siegel, J. D. Vieira, M. Viero, L. Wang, J. Wardlow, and J. Wheeler. HerMES: a search for high-redshift dusty galaxies in the HerMES Large Mode Survey – catalogue, number counts and early results. *Monthly Notices of the Royal Astronomical Society*, 462(2):1989–2000, 07 2016.

[18] Alan Bull, Barbara Andrews, Cristina Dorador, and Michael Goodfellow. Introducing the atacama desert. *Antonie van Leeuwenhoek*, 111, 05 2018.

[19] Samuel W. Hasinoff. *Photon, Poisson Noise*, pages 608–610. Springer US, Boston, MA, 2014.

[20] Rodney Loudon. Photon bunching and antibunching. *Physics Bulletin*, 27(1):21–23, jan 1976.

[21] Yoshiharu Asaki, Hiroshi Sudou, Yusuke Kono, Akihiro Doi, Richard Dodson, Nicolas Pradel, Yasuhiro Murata, Nanako Mochizuki, Philip G. Edwards, Tetsuo Sasao, and Edward B. Fomalont. Verification of the Effectiveness of VSOP-2 Phase Referencing with a Newly Developed Simulation Tool, ARIS. *Publications of the Astronomical Society of Japan*, 59(2):397–418, 04 2007.

[22] Tom Bakx and Stefanie Brackenhoff. deshima-dev/galspec: Update release, November 2020.

[23] Pauli Virtanen, Ralf Gommers, Travis E. Oliphant, Matt Haberland, Tyler Reddy, David Cournapeau, Evgeni Burovski, Pearu Peterson, Warren Weckesser, Jonathan Bright, Stéfan J. van der Walt, Matthew Brett, Joshua Wilson, K. Jarrod Millman, Nikolay Mayorov, Andrew R. J. Nelson, Eric Jones, Robert Kern, Eric Larson, C J Carey, İlhan Polat, Yu Feng, Eric W. Moore, Jake VanderPlas, Denis Laxalde, Josef Perktold, Robert Cimrman, Ian Henriksen, E. A. Quintero, Charles R. Harris, Anne M. Archibald, Antônio H. Ribeiro, Fabian Pedregosa, Paul van Mulbregt, and SciPy 1.0 Contributors. SciPy 1.0: Fundamental Algorithms for Scientific Computing in Python. *Nature Methods*, 17:261–272, 2020.

[24] Thomas L. Wilson and Guilloteau Stéphane. *Millimeter astronomy*. Springer, 2018.

[25] Deshima-Dev. deshima-dev/deshima-sensitivity: Sensitivity calculator for deshima-type spectrometers, 2020. `https://github.com/deshima-dev/deshima-sensitivity`.